

Infinite order accuracy limit of finite difference formulas in the complex plane

Bengt Fornberg *

Department of Applied Mathematics, University of Colorado, Boulder, CO 80309, USA

September 13, 2022

Abstract

It was recently found that finite difference (FD) formulas become remarkably accurate when approximating derivatives of analytic functions $f(z)$ in the complex $z = x + iy$ plane. On unit-spaced grids in the x, y -plane, the FD weights decrease to zero with the distance to the stencil center at a rate similar to that of a Gaussian, typically falling below the level of double precision accuracy $O(10^{-16})$ already about four node spacings away from the center point. We follow up on these observations here by analyzing and illustrating the features of such FD stencils in their infinite order accurate limit (for traditional FD approximations known as their pseudospectral limit).

Keywords: Finite differences, pseudospectral method, complex variables, analytic functions, Euler-Maclaurin.

Mathematics Subject Classification: Primary: 30-08, 30-E10, 65D25; Secondary: 30B40, 30E20, 65E99.

1 Introduction

Finite difference (FD) formulas have a long history, at first for interpolation and for solving ODEs, and later also for solving PDEs. It was noted in the early 1970's that the limit of FD stencils of increasing width / orders of accuracy is well defined. Also, if the limiting infinite order stencils are applied to periodic data, the result becomes identical to bringing the data to discrete Fourier space, differentiating it analytically, and then returning to physical space (giving rise to the expression pseudospectral (PS) approximations) [5, 7, 13].¹ PS methods quickly proved to be highly effective for tasks such as modeling nonlinear waves and turbulence.

Focusing on the core task of approximating derivatives using grid-based data, it was recently shown [10] that FD approximations for analytic functions $f(z)$ in the complex $z = x + iy$ plane offer great advantages in accuracy and locality over standard FD approximations for functions $f(x)$ with x

**Email:* fornberg@colorado.edu , ORCID 0000-0003-0014-6985

¹A different 'Chebyshev-PS' version, again utilizing the FFT, applies to non-periodic data discretized at the extremal points of Chebyshev polynomials [7, 19].

order of accuracy	weights										
2						$-\frac{1}{2}$	0	$\frac{1}{2}$			
4				$\frac{1}{12}$	$-\frac{2}{3}$	0	$\frac{2}{3}$	$-\frac{1}{12}$			
6			$-\frac{1}{60}$	$\frac{3}{20}$	$-\frac{3}{4}$	0	$\frac{3}{4}$	$-\frac{3}{20}$	$\frac{1}{60}$		
8		$\frac{1}{280}$	$-\frac{4}{105}$	$\frac{1}{5}$	$-\frac{4}{5}$	0	$\frac{4}{5}$	$-\frac{1}{5}$	$\frac{4}{105}$	$-\frac{1}{280}$	
10	$-\frac{1}{1260}$	$\frac{5}{504}$	$-\frac{5}{84}$	$\frac{5}{21}$	$-\frac{5}{6}$	0	$\frac{5}{6}$	$-\frac{5}{21}$	$\frac{5}{84}$	$-\frac{5}{504}$	$\frac{1}{1260}$
\vdots	\dots	\downarrow	\downarrow	\downarrow	\downarrow	\vdots	\downarrow	\downarrow	\downarrow	\downarrow	\dots
limit	\dots	$\frac{1}{4}$	$-\frac{1}{3}$	$\frac{1}{2}$	-1	0	1	$-\frac{1}{2}$	$\frac{1}{3}$	$-\frac{1}{4}$	\dots

Table 1: Weights for centered FD approximations of the first derivative on a grid with spacing h (omitting the factor $1/h$).

real. The purpose of this present study is to introduce and analyze corresponding complex plane PS approximations.

After a brief review of FD and PS approximations with a real-valued independent variable x in Section 2.1 and FD approximations with a complex-valued independent variable z in Section 2.2, we turn the attention to PS methods in the complex plane. The complex plane PS limit for derivative approximations is introduced in Section 3, followed in Section 4 by a discussion of convergence rates, and the influence of the order of the approximated derivative. Section 5 focuses on interpolation and Section 6 provides some numerical illustrations. This is followed by Conclusions and References.

All numerical calculations in this work were carried out in MATLAB together with the Advanpix extended precision toolbox².

2 Some background on FD and PS methods

2.1 FD and PS approximations with real-valued independent variable x

Although the data in Tables 1 and 2 has been given previously, we show it again here to illustrate the limit process that we will generalize to the complex plane. With nodes unit-spaced along a line: $x_k = k$, $k = 0, \pm 1, \pm 2, \dots$, the limiting FD weights w_k decay in magnitude to zero as $O(1/k)$ and $O(1/k^2)$ for odd and even order of derivatives, respectively.

While PS methods have proven extremely effective in numerous applications, the slow algebraic decay rate of the weights with the distance from the stencil center point is problematic, since a derivative is a completely local property of a function, and should not depend heavily on far-away function values.

²Advanpix, Multiprecision Computing Toolbox for MATLAB, <http://www.advanpix.com/>, Advanpix LLC., Yokohama, Japan.

order of accuracy		weights									
2					1	-2	1				
4				$-\frac{1}{12}$	$\frac{4}{3}$	$-\frac{5}{2}$	$\frac{4}{3}$	$-\frac{1}{12}$			
6			$\frac{1}{90}$	$-\frac{3}{20}$	$\frac{3}{2}$	$-\frac{49}{18}$	$\frac{3}{2}$	$-\frac{3}{20}$	$\frac{1}{90}$		
8		$-\frac{1}{560}$	$\frac{8}{315}$	$-\frac{1}{5}$	$\frac{8}{5}$	$-\frac{205}{72}$	$\frac{8}{5}$	$-\frac{1}{5}$	$\frac{8}{315}$	$-\frac{1}{560}$	
10	$\frac{1}{3150}$	$-\frac{5}{1008}$	$\frac{5}{126}$	$-\frac{5}{21}$	$\frac{5}{3}$	$-\frac{5269}{1800}$	$\frac{5}{3}$	$-\frac{5}{21}$	$\frac{5}{126}$	$-\frac{5}{1008}$	$\frac{1}{3150}$
\vdots	\cdots	$\downarrow n$	\downarrow	\downarrow	\downarrow	\downarrow	\downarrow	\downarrow	\downarrow	\downarrow	\cdots
limit	\cdots	$-\frac{2}{4^2}$	$\frac{2}{3^2}$	$-\frac{2}{2^2}$	$\frac{2}{1^2}$	$-\frac{\pi^2}{3}$	$\frac{2}{1^2}$	$-\frac{2}{2^2}$	$\frac{2}{3^2}$	$-\frac{2}{4^2}$	\cdots

Table 2: Weights for centered FD approximations of the second derivative (omitting the factor $1/h^2$).

2.2 FD approximations with complex-valued independent variable z

This section recalls briefly some of the main observations from [10]. Functions $f(z)$ with $z = x + iy$ are *analytic* if $\frac{df}{dz} = \lim_{\Delta z \rightarrow 0} \frac{f(z+\Delta z)-f(z)}{\Delta z}$ is uniquely defined, no matter from which direction in the complex plane Δz approaches zero.³ An important consequence is the Cauchy-Riemann equations. Separating into real and imaginary parts, $z = x + iy$ and $f(z) = u(x, y) + i v(x, y)$, these are

$$\frac{\partial u}{\partial x} = \frac{\partial v}{\partial y}, \quad \frac{\partial v}{\partial x} = -\frac{\partial u}{\partial y}. \quad (1)$$

Analyticity is assumed for all functions that the present FD and PS complex plane approximations are to be applied to.

Table 3 forms a complex plane counterpart to the top two lines in Tables 1 and 2. With grid spacing h , the order of accuracy for the shown 3×3 stencils are $O(h^8)$ and $O(h^7)$, and for the 5×5 stencils $O(h^{24})$ and $O(h^{23})$, respectively.

A major difference from the traditional FD cases is that complex plane FD weights decrease in magnitude with the distance from the stencil much faster. With stencil nodes at $z_k = \mu + i\nu$, $-n \leq \mu, \nu \leq +n$ (i.e., $k = 1, 2, \dots, (2n+1)^2$), the decay rate contains again an algebraic factor, but now further multiplied by the extremely rapidly decreasing factor $e^{-\frac{\pi}{2}(\mu^2 + \nu^2)}$. This makes the approximations remain highly localized even when their stencil sizes / accuracy orders increase indefinitely.

With the node set just described, we define

$$\sigma_n(z) = z \prod_{\mu, \nu = -n}^n ' \left(1 - \frac{z}{\mu + i\nu} \right), \quad (2)$$

where the prime indicates that, in the double product over μ and ν , the case $\mu = \nu = 0$ is omitted. Except for the node z_k that is located at the origin, the weights w_k for the first derivative then

³This provides a heuristic insight into the high accuracy of complex plane FD formulas. To approximate, say $\frac{d}{dx}$, nodes need not be strung out along the x -axis, but can for $\frac{d}{dz}$ remain much more local, using information from every direction surrounding the approximation point.

Stencil size 3×3

Stencil size 5×5

$$\begin{aligned}
 f'(0) &\approx \frac{1}{40h} \begin{bmatrix} -1-i & -8i & 1-i \\ -8 & 0 & 8 \\ -1+i & 8i & 1+i \end{bmatrix} f; & \frac{1}{h} \begin{bmatrix} \frac{1+i}{477360} & \frac{4(-1-i)}{29835} & \frac{i}{1326} & \frac{4(1-i)}{29835} & \frac{-1+i}{477360} \\ \frac{4(-1-i)}{29835} & \frac{8(-1-i)}{351} & \frac{-8i}{39} & \frac{8(1-i)}{351} & \frac{4(1-i)}{29835} \\ \frac{1}{1326} & \frac{-8}{39} & 0 & \frac{8}{39} & \frac{-1}{1326} \\ \frac{4(-1+i)}{29835} & \frac{8(-1+i)}{351} & \frac{8i}{39} & \frac{8(1+i)}{351} & \frac{4(1+i)}{29835} \\ \frac{1-i}{477360} & \frac{4(-1+i)}{29835} & \frac{-i}{1326} & \frac{4(1+i)}{29835} & \frac{-1-i}{477360} \end{bmatrix} f \\
 f''(0) &\approx \frac{1}{20h^2} \begin{bmatrix} i & -8 & -i \\ 8 & 0 & 8 \\ -i & -8 & i \end{bmatrix} f; & \frac{1}{h^2} \begin{bmatrix} \frac{-i}{477360} & \frac{8(-1+3i)}{149175} & \frac{1}{1326} & \frac{8(-1-3i)}{149175} & \frac{i}{477360} \\ \frac{8(1+3i)}{149175} & \frac{16i}{351} & \frac{-16}{39} & \frac{-16i}{351} & \frac{8(1-3i)}{149175} \\ \frac{-1}{1326} & \frac{16}{39} & 0 & \frac{16}{39} & \frac{-1}{1326} \\ \frac{8(1-3i)}{149175} & \frac{-16i}{351} & \frac{-16}{39} & \frac{16i}{351} & \frac{8(1+3i)}{149175} \\ \frac{i}{477360} & \frac{8(-1-3i)}{149175} & \frac{1}{1326} & \frac{8(-1+3i)}{149175} & \frac{-i}{477360} \end{bmatrix} f
 \end{aligned}$$

Table 3: The weights in 3×3 and 5×5 size stencils for the first two derivatives.

become

$$w_k = -\frac{1}{z_k} \sigma'_n(0) / \sigma'_n(z_k), \quad (3)$$

and for the p^{th} derivative

$$w_k = -p! \left(\sum_{m=1}^p \frac{1}{m! z_k^{p-m+1}} \sigma_n^{(m)}(0) \right) / \sigma'_n(z_k). \quad (4)$$

Equations (3), (4) hold for arbitrary node distributions z_k (as long as one node is at the origin and $z_k \neq 0$). For the lattice-based square node layouts considered here, $\sigma_n^{(m)}(0) = 0$ unless $m = 1, 5, 9, 13, \dots$, making three out of every 4 terms vanish in the sum (4).⁴ The ratios $\sigma_n^{(m)}(0) / \sigma'_n(z_k)$, appearing in (4), will next be analyzed in the $n \rightarrow \infty$ limit.

3 The PS limit of $n \rightarrow \infty$

Equations (3), (4) showed that complex plane FD weights are described by the $\sigma_n(z)$ function, introduced in (2). In the $n \rightarrow \infty$ limit, $\sigma_n(z)$ converges to the Weierstrass σ -function, which typically is defined as

$$\sigma(z) = z \prod_{\mu, \nu=-\infty}^{\infty} ' \left(\left(1 - \frac{z}{\mu + i\nu} \right) e^{z/(\mu+i\nu) + \frac{1}{2}(z/(\mu+i\nu))^2} \right). \quad (5)$$

The exponential factor serves only the purpose of making the product convergent (and to the same value) irrespective of the order of its factors, but is unnecessary when ordering these from the origin and outwards⁵. By its construction, $\sigma(z)$ has simple zeros at all Gaussian integers $z = \mu + i\nu$, μ, ν

⁴The formulas (3), (4) (following from Lagrange's interpolation formula) will be used for theoretical analysis. The two algorithms denoted Methods 1 and 2, respectively, in [10], are more practical computationally.

⁵By symmetries, it holds that $\prod_{\mu, \nu=-n}^n ' e^{z/(\mu+i\nu) + \frac{1}{2}(z/(\mu+i\nu))^2} = 1$ for all $n = 1, 2, 3, \dots$

integers, and is normalized by $\sigma'(0) = 1$.

It was shown in [10], Appendix 3 (without reference to established theory for the $\sigma(z)$ function) that

$$\lim_{n \rightarrow \infty} |\sigma'_n(0) / \sigma'_n(z_k)| = e^{-\frac{\pi}{2} |z_k|^2} = e^{-\frac{\pi}{2} (\mu^2 + \nu^2)}, \quad (6)$$

where $z_k = \mu + i\nu$ is a Gaussian integer node within the size n stencil. Together with (4), this sufficed for establishing the Gaussian-type coefficient decay mentioned above.⁶ The rest of the present paper extends on this result.

In order to obtain the PS weights for the p^{th} derivative by means of (4), two further results are needed:

1. Sharpen (6) to obtain the value for $\sigma'(0)/\sigma'(z_k)$, i.e., not just its magnitude, and
2. Determine the constants $\sigma^{(m)}(0)/\sigma'(0)$, $m = 1, 5, 9, \dots$ up through $m \leq p$, i.e., the coefficients in the Taylor expansion of $\sigma(z)$ around $z = 0$.

The next two subsections address these issues in turn.

3.1 Refinement of (6)

It follows from (6) that

$$\sigma'(0) / \sigma'(z_{\mu+i\nu}) = \lambda_{\mu,\nu} e^{-\frac{\pi}{2} (\mu^2 + \nu^2)}, \quad (7)$$

with $|\lambda_{\mu,\nu}| = 1$. By using results from [18], Chapter 23, it furthermore follows that $\lambda_{\mu,\nu} = (-1)^{\mu+\nu+\mu\nu}$ (the key first step is to re-express the $z \rightarrow 0$ limit in (23.2.17) by L'Hôpital's rule). This implies the sign pattern for $\lambda_{\mu,\nu}$ over the nodes $z_k = \mu + i\nu$ as shown in Figure 1 (a) (i.e., $\lambda_{\mu,\nu} = +1$ if both μ and ν are divisible by 2, and $= -1$ otherwise).

3.2 Taylor expansion of the Weierstrass σ -function

The Taylor expansion of $\sigma(z)$ is known in the literature. The results quoted next can be found in [18], Chapter 23, with additional perspectives provided in [3], Section 3.4. The *Weierstrass invariants* $\{g_2, g_3\}$ corresponding to the lattice periods $\{1, i\}$ take the values $g_2 = \Gamma(\frac{1}{4})^8 / (16\pi^2) \approx 189.072720$ and $g_3 = 0$. The Taylor expansion of $\sigma(z)$ around $z = 0$ becomes

$$\sigma(z) = z [1 + r_1 (g_2 z^4)^1 + r_2 (g_2 z^4)^2 + r_3 (g_2 z^4)^3 + \dots], \quad (8)$$

where r_i are rational numbers, available via recursions ([18], equation (23.9.7)).⁷ Alternatively, symbolic algebra systems readily provide these coefficients. For example the Mathematica statement

```
Series[WeierstrassSigma[z, {g2, 0}], {z, 0, 24}]
```

⁶The decay comes from the very rapid growth of $\sigma'_n(z_k)$, and in view of (4) therefore applies to any order derivative.

⁷The recursion produces an array of coefficients $a_{m,n}$, $m, n = 0, 1, 2, \dots$ (using integer arithmetic only, implying no stability issues). Since $g_3 = 0$, we need only to retain the entries $a_{m,0}$, $m = 0, 1, 2, \dots$, from which the expansion shown in (9) then follows.

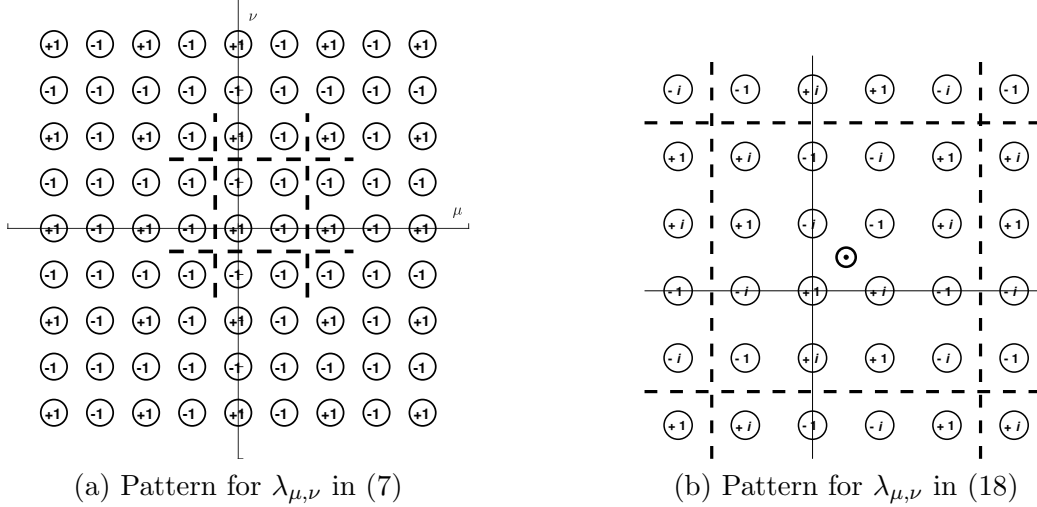


Figure 1: The pattern for the variable $\lambda_{\mu,\nu}$ (satisfying $|\lambda_{\mu,\nu}| = 1$) displayed over the μ, ν lattice in two cases: (a): As used in equation (7), and (b): As used in equation (18). In this latter case, the interpolation point is marked by \odot , matching the notation in (12), (13). In both cases, the dashed square marks a region that repeats indefinitely across the full complex plane.

produces the output

$$z - \frac{g2 z^5}{240} - \frac{g2^2 z^9}{161280} + \frac{23 g2^3 z^{13}}{16605388800} - \frac{107 g2^4 z^{17}}{186999616512000} + \frac{851 g2^5 z^{21}}{8650318251294720000} + O[z]^{25}, \quad (9)$$

from which we read off $r_1 = -\frac{1}{240}$, $r_2 = -\frac{1}{161280}$, etc. Combined with (4) and (7), this provides the PS weights for the p^{th} derivative.

3.3 Examples of PS derivative approximations

From the results above, we can explicitly write down the complex plane PS weights for any derivative. Following up on the FD cases shown in Table 3, we show in Table 4 the central 7×7 area of the PS approximations for $f'(0)$ and $f''(0)$. For any order derivative, all weights take the form of a rational complex number multiplied by $e^{-\frac{\pi}{2}(\mu^2 + \nu^2)}$. Already at the corner positions shown in Table 4, this factor has decreased to $e^{-\frac{\pi}{2}(3^2 + 3^2)} \approx 5 \cdot 10^{-13}$.⁸

Compared to real-valued PS approximations in two independent variables x, y , the situation with $z = x + iy$ and $f(z)$ analytic is vastly different. One can heuristically note that complex PS stencils get their rapid decay in weights by effectively utilizing the fact that they will only be applied to functions obeying the Cauchy-Riemann equations (1). Although these equations hold for all analytic functions, this is still a small subset of all functions of two variables.⁹

⁸Using double precision, weights in magnitude less than 10^{-16} can be set to zero, with dual benefits: (i) functions the approximation is applied to need to be smooth only within the extent of the stencil, and (ii) it is unnecessary to decide on which approximation order to use (as long as the truncated PS stencil size is acceptable).

⁹For example, an analytic function can never have a finite local maximum or minimum point in either its real or imaginary part. It is also uniquely determined everywhere if it is known just along any finite curve segment, no matter how short. Many additional notable features are described in complex variables textbooks, for ex., [2, 11].

First derivative

$$\frac{1}{h} \begin{bmatrix} \vdots & \vdots \\ \dots & \frac{-1-i}{6} & \frac{-2-3i}{13} & \frac{-1-3i}{10} & \frac{-i}{3} & \frac{1-3i}{10} & \frac{2-3i}{13} & \frac{1-i}{6} & \dots \\ \dots & \frac{-3-2i}{13} & \frac{1+i}{4} & \frac{-1-2i}{5} & \frac{i}{2} & \frac{1-2i}{5} & \frac{-1+i}{4} & \frac{3-2i}{13} & \dots \\ \dots & \frac{-3-i}{10} & \frac{-2-i}{5} & \frac{-1-i}{2} & -i & \frac{1-i}{2} & \frac{2-i}{5} & \frac{3-i}{10} & \dots \\ \dots & \frac{-1}{3} & \frac{1}{2} & -1 & 0 & 1 & \frac{-1}{2} & \frac{1}{3} & \dots \\ \dots & \frac{-3+i}{10} & \frac{-2+i}{5} & \frac{-1+i}{2} & i & \frac{1+i}{2} & \frac{2+i}{5} & \frac{3+i}{10} & \dots \\ \dots & \frac{-3+2i}{13} & \frac{1-i}{4} & \frac{-1+2i}{5} & \frac{-i}{2} & \frac{1+2i}{5} & \frac{-1-i}{4} & \frac{3+2i}{13} & \dots \\ \dots & \frac{-1+i}{6} & \frac{-2+3i}{13} & \frac{-1+3i}{10} & \frac{i}{3} & \frac{1+3i}{10} & \frac{2+3i}{13} & \frac{1+i}{6} & \dots \\ \vdots & \vdots \end{bmatrix}$$

Second derivative

$$\frac{1}{h^2} \begin{bmatrix} \vdots & \vdots \\ \dots & \frac{i}{9} & \frac{-10+24i}{169} & \frac{-4+3i}{25} & \frac{-2}{9} & \frac{-4-3i}{25} & \frac{-10-24i}{169} & \frac{-i}{9} & \dots \\ \dots & \frac{10+24i}{169} & \frac{-i}{4} & \frac{-6+8i}{25} & \frac{1}{2} & \frac{-6-8i}{25} & \frac{i}{4} & \frac{10-24i}{169} & \dots \\ \dots & \frac{4+3i}{25} & \frac{6+8i}{25} & i & -2 & -i & \frac{6-8i}{25} & \frac{4-3i}{25} & \dots \\ \dots & \frac{2}{9} & \frac{-1}{2} & 2 & 0 & 2 & \frac{-1}{2} & \frac{2}{9} & \dots \\ \dots & \frac{4-3i}{25} & \frac{6-8i}{25} & -i & -2 & i & \frac{6+8i}{25} & \frac{4+3i}{25} & \dots \\ \dots & \frac{10-24i}{169} & \frac{i}{4} & \frac{-6-8i}{25} & \frac{1}{2} & \frac{-6+8i}{25} & \frac{-i}{4} & \frac{10+24i}{169} & \dots \\ \dots & \frac{-i}{9} & \frac{-10-24i}{169} & \frac{-4-3i}{25} & \frac{-2}{9} & \frac{-4+3i}{25} & \frac{-10+24i}{169} & \frac{i}{9} & \dots \\ \vdots & \vdots \end{bmatrix}$$

Table 4: Central 7×7 area of the PS stencils for the first two derivatives. The node locations are $z_k = \mu + i\nu$, with μ and ν integers. Each of the numbers shown should be multiplied by $e^{-\frac{\pi}{2}(\mu^2 + \nu^2)}$ to obtain the actual PS weight.

n	1 st derivative			
	Weight at $1 + i$ position		Weight at $4 + 3i$ position	
1	0.02500000	-0.02500000 i	-	-
2	0.02279202	-0.02279202 i	-	-
3	0.02220318	-0.02220318 i	-	-
4	0.02196561	-0.02196561 i	(-7.949076 -13.68542 i)	$\cdot 10^{-18}$
5	0.02184638	-0.02184638 i	(-0.138855 -7.594808 i)	$\cdot 10^{-18}$
6	0.02177811	-0.02177811 i	(1.273456 -4.837222 i)	$\cdot 10^{-18}$
7	0.02173538	-0.02173538 i	(1.594705 -3.509363 i)	$\cdot 10^{-18}$
\vdots	\downarrow	\downarrow	\downarrow	\downarrow
Limit	0.02160696	-0.02160696 i	(1.410638 -1.057978 i)	$\cdot 10^{-18}$

n (Gaussian integer)	8 th derivative			
	Weight at $1 + i$ position		Weight at $4 + 3i$ position	
1	$5.040000 \cdot 10^{+2}$	0 i	-	-
2	$4.707331 \cdot 10^{+2}$	0 i	-	-
3	$4.614927 \cdot 10^{+2}$	0 i	-	-
4	$4.577448 \cdot 10^{+2}$	0 i	(25.385237 -31.01112 i)	$\cdot 10^{-16}$
5	$4.558591 \cdot 10^{+2}$	0 i	(17.915851 -7.091375 i)	$\cdot 10^{-16}$
6	$4.547780 \cdot 10^{+2}$	0 i	(12.635851 -1.283046 i)	$\cdot 10^{-16}$
7	$4.541008 \cdot 10^{+2}$	0 i	(9.771112 0.664519 i)	$\cdot 10^{-16}$
\vdots	\downarrow	\downarrow	\downarrow	\downarrow
Limit	$4.520631 \cdot 10^{+2}$	0 i	(3.782035 2.417118 i)	$\cdot 10^{-16}$

Table 5: Some weights when approximating the 1st and the 8th derivative with stencils of increasing size. The analytic limits in the two 1st derivative cases are $\frac{1-i}{2} e^{-\pi}$ and $\frac{4-3i}{25} e^{-25\pi/2}$, and in the two 8th derivative cases $42(60 + g2) e^{-\pi}$ and $\frac{-168}{(1+2i)^8} \left(\frac{48(2+i)}{(1+2i)^7} - i g2 \right) e^{-25\pi/4}$ with, as before, $g2 = \Gamma\left(\frac{1}{4}\right)^8 / (16\pi^2)$.

4 Convergence / divergence illustrations when varying order of accuracy and order of derivative

4.1 Derivatives of fixed orders

Table 5 provides further illustrations of the results above. For any fixed order derivative, weights for increasing n are seen to approach the predicted $n \rightarrow \infty$ limits.

4.2 Derivatives of increasing orders

We see also in Table 5 that, as derivative orders increase, the weights get larger, with the weights for the 8th derivative about 200 times larger than those for the 1st derivative (however, still decreasing as predicted with increasing distance from the stencil center). To put this growth in some perspective, we consider next the corresponding growth in the case of traditional PS methods.

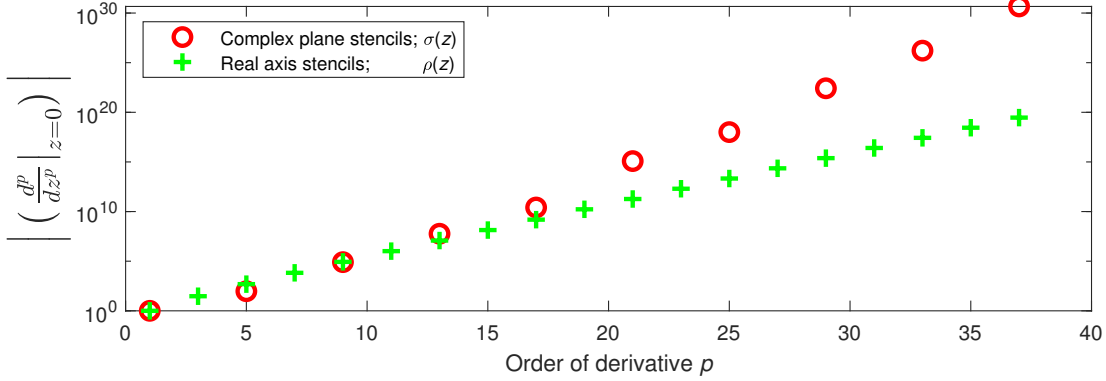


Figure 2: The growths of $|\sigma^{(p)}(0)|$ and $|\rho^{(p)}(0)|$ with the derivative order p when the stencil nodes are on a unit-spaced infinite lattice in the complex plane versus along the real axis, respectively (evaluating to zero where not shown).

The counterpart function to (5) for centered stencils with nodes only along the real axis is¹⁰

$$\rho(z) = z \prod_{\mu=-\infty}^{\infty} \left(1 - \frac{z}{\mu}\right) = \frac{\sin \pi z}{\pi} = z - \frac{\pi^2}{3!} z^3 + \frac{\pi^4}{5!} z^5 - \frac{\pi^6}{7!} z^7 + \frac{\pi^8}{9!} z^9 - \frac{\pi^{10}}{11!} z^{11} + \dots \quad (10)$$

Based on the coefficients in (9) and (10), Figure 2 compares the growths of $|\sigma^{(p)}(0)|$ and $|\rho^{(p)}(0)|$ with p in the cases of complex plane and real axis PS stencils (reflecting the growth of PS weights). While for a fixed order derivative, the weights decay much faster with node distance from the origin in the complex plane stencil case (thanks to the $e^{-\frac{\pi}{2}(\mu^2+\nu^2)}$ factor), the weights for nodes near to the origin grow in magnitude faster with derivative order p in the complex plane PS case. If one wishes to approximate very high order derivatives based on complex plane data, this growth becomes problematic, and Cauchy integral-type methods [6, 15, 16] might be preferable over complex plane FD stencils.

4.3 Derivatives of unbounded orders - The Euler-Maclaurin formula

The growth in weights with the order of the derivative that is approximated somewhat limits the range of applications for which it is beneficial to use the PS $n \rightarrow \infty$ limit. This is illustrated here in the case of the Euler-Maclaurin formula. This can be written as

$$\int_0^\infty f(x) dx - h \sum_{k=0}^\infty f(kh) + \frac{h}{2} f(0) = h \left[\frac{h}{12} f^{(1)}(0) - \frac{h^3}{720} f^{(3)}(0) + \frac{h^5}{30240} f^{(5)}(0) - \dots \right]. \quad (11)$$

In the bracket of the right hand side, the powers of h get exactly canceled by the powers of h in the denominators of the derivative approximations, making this expression independent of h . Choosing as before stencils with $z_k = \mu + i\nu$, $-n \leq \mu, \nu \leq +n$ allows for $n = 1$ (3×3 stencils) the inclusion of terms up through $f^{(7)}(0)$, for $n = 2$ up through $f^{(23)}(0)$, for $n = 3$ up through $f^{(47)}(0)$, etc.

The stencil weights in the $n = 1$ and $n = 2$ cases are numerically very small (thanks to the rapid rate the coefficients in (11) go to zero). They were given in closed form in [8], and there shown

¹⁰omitting an extra exponential factor in the product that would ensure absolute convergence

n	Euler Maclaurin weights			
	Weight at $1 + i$ position		Weight at $4 + 3i$ position	
1	0.002036	-0.001932 i	-	-
2	0.001975	-0.001681 i	-	-
3	-7.200552	-6.679490 i	-	-
4	(4.6637	+4.5444 i) $\cdot 10^{11}$	0.002260	-0.003205 i
5	(-1.7182	-1.6989 i) $\cdot 10^{29}$	(-6.7779	+2.6158 i) $\cdot 10^{14}$
\vdots	\downarrow	\downarrow	\downarrow	\downarrow
Limit	Does not exist		Does not exist	

Table 6: Some weights when approximating the Euler-Maclaurin operator with stencils of increasing size.

to provide excellent accuracy for (11), as was the $n = 3$ case in Figure 6 of [9]. However, due to the very high order derivatives that enter for larger n values together with the rapid growth in weights with the order¹¹, the resulting Euler-Maclaurin weights grow very rapidly as n is increased further, as seen in Table 6 (using the same format as in Table 5). While accurate results still can be obtained with use of extended precision arithmetic, the PS limit of $n \rightarrow \infty$ does not exist.

5 PS formulas for interpolation

A common task when given data on an equi-spaced grid is to interpolate to in-between grid point locations. The discussion in [10], Section 7, was limited to the case of interpolating to the center location between adjacent rows and columns. This suffices for interpolating to a twice as dense grid, since turning such a stencil 45° will allow all values on the finer grid to be filled in. The simplest such interpolation stencil can be written as

$$f(\odot) = \frac{1}{4} \begin{bmatrix} 1 & \odot & 1 \\ 1 & & 1 \end{bmatrix} f + O(h^4), \quad (12)$$

where \odot marks the center of a local square on the coarse grid. The next size stencil of this type was also given explicitly in [10]:

$$f(\odot) = \frac{1}{106496} \begin{bmatrix} -25 & 162 - 459i & 162 + 459i & -25 \\ 162 + 459i & 26325 & 26325 & 162 - 459i \\ 162 - 459i & 26325 & \odot & 26325 & 162 + 459i \\ -25 & 162 + 459i & 162 - 459i & -25 \end{bmatrix} f + O(h^{16}). \quad (13)$$

To set the background for deriving the PS limit of these interpolation formulas, we start by considering the real-valued case.

5.1 PS interpolation in the real-valued case

The concept for finding interpolation weights is illustrated in Figure 3 in the case of unit-spaced nodes at $x_k = k$, $k = -n, \dots, -1, 0, 1, \dots, n$ for the case of $n = 5$. The successive curves show the polynomials that interpolate data that is zero at all nodes apart from taking the value one

¹¹Following from the growth of $\sigma^{(p)}(0)$ with p , as shown in Figure 2

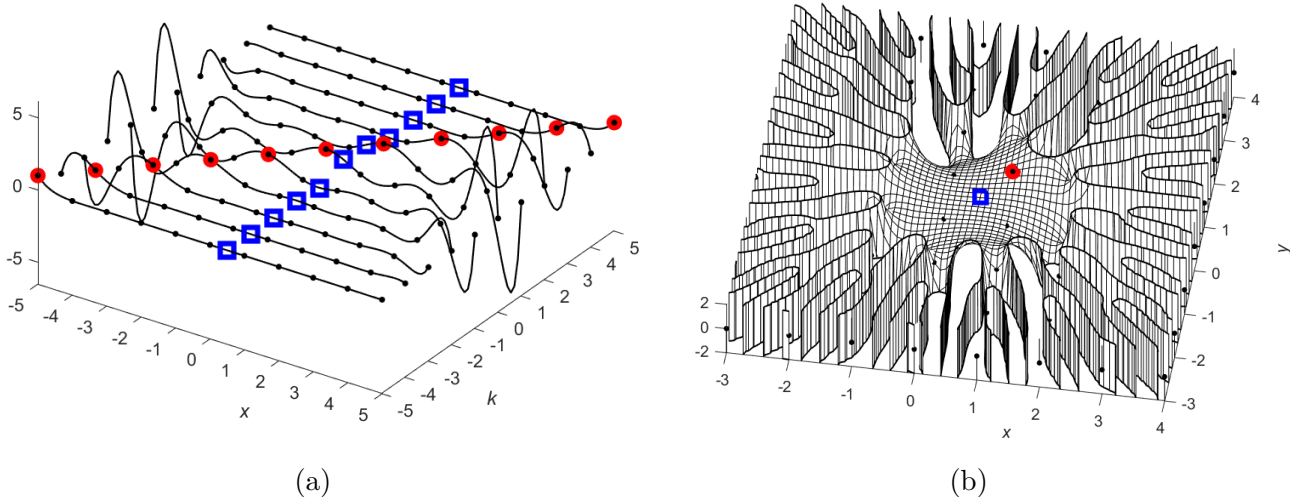


Figure 3: Polynomials that take the value one at one node point, and zero at all the other ones (a) Nodes $x_k = k$, $k = -5, \dots, +5$; eleven cases and (b) Nodes $z_k = \mu + i\nu$, $-3 \leq \mu, \nu \leq 4$; real part of the interpolation polynomial that is zero at all these nodes apart from taking the value one at $z = 1 + i$. The blue square at $x = \frac{1}{2}$ and $z = \frac{1}{2}(1 + i)$, respectively, illustrate an example of a location at which we want to interpolate.

at node $x = k$ (as marked with red circles). Reading off the values of these polynomials at some intermediate x -location (in the figure shown by blue squares at $x = \frac{1}{2}$) gives the *weights* to use at the x_k locations when interpolating from the $f(k)$ values to approximate $f(\frac{1}{2})$.

In the limit of $n \rightarrow \infty$, it follows from Lagrange's interpolation formula, together with (10), that the weights w_k interpolating at $x = \xi$ become

$$w_k = \frac{\sin \pi \xi}{\pi(\xi - x_k)} (-1)^k = \frac{\rho(\xi)}{\xi - x_k} (-1)^k. \quad (14)$$

As to be expected, in the limit of $\xi \rightarrow x_k$, the weights become one at this node x_k , and zero at all other nodes. Interpolating to the half-way point $\xi = \frac{1}{2}$ gives

$$w_k = \frac{(-1)^k}{\pi(\frac{1}{2} - k)}. \quad (15)$$

Much as for PS derivative approximations along the real axis, the decay of $|w_k|$ with $|k|$ is very slow.

5.2 PS interpolation in the complex-valued case

In the real-valued case described just above, it would have made no difference if we, instead of letting the nodes be located at $x_k = k$, $k = -n, \dots, -1, 0, 1, \dots, n$, had included one more node to the right, at $k = n + 1$ (making the total node count even), when taking the limit of $n \rightarrow \infty$. Equations (14) and (15) are obtained in either case. Due to the extremely rapid growth of $\sigma(z)$

with $|z|$, this is not the case with z complex. Interpolation is naturally done to locations within a local grid square with stencils centered around this square (as illustrated in (12), (13)). We therefore focus next on square stencils with an even number of nodes. Including also one single strip of nodes immediately above and to the right of an odd-numbered square node set $z_k = \mu + i\nu$, $-n \leq \mu, \nu \leq n$ makes the exponential factors in (5) no longer cancel, but contribute (in the $n \rightarrow \infty$ limit) an extra factor of $e^{\frac{\pi}{2}(1-i)(1+z)}$.¹² Some further algebra will then show that the function

$$\tau(z) = \sigma(z) e^{-\frac{\pi}{2}(1-i)(2+z)} \quad (16)$$

becomes a counterpart to $\sigma(z)$, again with simple zeros at all integer lattice points, but now symmetric around $z = \frac{1}{2}(1+i)$ rather than for $\sigma(z)$ around $z = 0$ (in the sense that its Taylor expansion around this point contains only terms with powers of $z - \frac{1}{2}(1+i)$ evenly divisible by four).¹³

5.2.1 Case when interpolating to the center-point of a grid square

Figure 3 (b) shows the real part of the complex plane counterpart to a single curve in Figure 3 (a), i.e., the interpolating polynomial which is zero at all nodes $z_k = \mu + i\nu$, $-n \leq \mu, \nu \leq n+1$ (here with $n = 3$) apart from at one node point z_k (here shown at $1+i$) where it equals one. Just as in the 1-D case, we read off the interpolating weight to be used at z_k as the value of this polynomial at the $z = \xi$ location (again marked with a blue square, here shown at $\xi = \frac{1}{2}(1+i)$). This node set is symmetric with regard to its central square $[0, 1] \times [0, 1]$, within which we want to interpolate based on function values at the nodes.

The PS limit corresponds, as before, to letting $n \rightarrow \infty$. To find this limit in closed form, we obtain from σ -function identities

$$\tau\left(\frac{1}{2}(1+i)\right) = -c(1+i) \quad \text{where} \quad c = \frac{2e^{-5\pi/4}\sqrt{\pi}}{\Gamma(\frac{1}{4})^2} \approx 0.0053134, \quad (17)$$

and for μ, ν integers

$$\lim_{z \rightarrow \mu + i\nu} \frac{\tau(z)}{z - (\mu + i\nu)} = -\lambda_{\mu,\nu} e^{\frac{\pi}{2}((\mu-\frac{1}{2})^2 + (\nu-\frac{1}{2})^2 - \frac{5}{2})}, \quad (18)$$

with the unit-magnitude coefficients $\lambda_{\mu,\nu} = i^{2\mu\nu - \mu + \nu}$ graphically illustrated in Figure 1 (b).

From these last two equations follows that the PS interpolation weight w_k at grid point $z_k = \mu + i\nu$ becomes

$$w_k = \frac{c(1+i)}{(\frac{1}{2}(1+i) - (\mu + i\nu)) \lambda_{\mu,\nu}} e^{-\frac{\pi}{2}((\mu-\frac{1}{2})^2 + (\nu-\frac{1}{2})^2 - \frac{5}{2})}. \quad (19)$$

Table 7 gives PS weights over an 8×8 node set surrounding the interpolation point, and Table 8 shows the convergence of two of the FD weights, as the PS limit is approached.

¹²As can be shown with an argument similar to the one in [10], Appendix C, or deduced from σ -function identities in [18], Section 23.2.

¹³Similar to how the Taylor expansion of $\sigma(z)$ around $z = 0$ only has terms with powers of z giving remainder 1 when divided by four, c.f., (8), (9).

$$f(\odot) \approx \begin{bmatrix} \vdots & \vdots \\ \dots & \frac{-2}{7} & \frac{2-12i}{37} & \frac{10+4i}{29} & \frac{-6+8i}{25} & \frac{-6-8i}{25} & \frac{10-4i}{29} & \frac{2+12i}{37} & \frac{-2}{7} & \dots \\ \dots & \frac{2+12i}{37} & \frac{2}{5} & \frac{2-8i}{17} & \frac{-6-4i}{13} & \frac{-6+4i}{13} & \frac{2+8i}{17} & \frac{2}{5} & \frac{2-12i}{37} & \dots \\ \dots & \frac{10-4i}{29} & \frac{2+8i}{17} & \frac{-2}{3} & \frac{2-4i}{5} & \frac{2+4i}{5} & \frac{-2}{3} & \frac{2-8i}{17} & \frac{10+4i}{29} & \dots \\ \dots & \frac{-6-8i}{25} & \frac{-6+4i}{13} & \frac{2+4i}{5} & 2 & 2 & \frac{2-4i}{5} & \frac{-6-4i}{13} & \frac{-6+8i}{25} & \dots \\ \dots & \frac{-6+8i}{25} & \frac{-6-4i}{13} & \frac{2-4i}{5} & 2 & 2 & \frac{2+4i}{5} & \frac{-6+4i}{13} & \frac{-6-8i}{25} & \dots \\ \dots & \frac{10+4i}{29} & \frac{2-8i}{17} & \frac{-2}{3} & \frac{2+4i}{5} & \frac{2-4i}{5} & \frac{-2}{3} & \frac{2+8i}{17} & \frac{10-4i}{29} & \dots \\ \dots & \frac{2-12i}{37} & \frac{2}{5} & \frac{2+8i}{17} & \frac{-6+4i}{13} & \frac{-6-4i}{13} & \frac{2-8i}{17} & \frac{2}{5} & \frac{2+12i}{37} & \dots \\ \dots & \frac{-2}{7} & \frac{2+12i}{37} & \frac{10-4i}{29} & \frac{-6-8i}{25} & \frac{-6+8i}{25} & \frac{10+4i}{29} & \frac{2-12i}{37} & \frac{-2}{7} & \dots \\ \vdots & \vdots \end{bmatrix} f$$

Table 7: PS interpolation weights in the central 8×8 node area on a unit-spaced grid when interpolating to the grid center point $z_c = \frac{1}{2} + \frac{i}{2}$, marked by \odot . The displayed numbers need further, at the node $z_k = \mu + i\nu$, be multiplied by $c \cdot e^{-\frac{\pi}{2}((\mu-\frac{1}{2})^2 + (\nu-\frac{1}{2})^2 - \frac{5}{2})}$, where the constant c is defined in (17).

n	Interpolation		
	Weight at $1 + i$ position	Weight at $4 + 3i$ position	
0	0.250000	-	-
1	0.247192	-	-
2	0.246481	-	-
3	0.246232	$(-7.22388 - 4.91727 i) \cdot 10^{-14}$	
4	0.246166	$(-2.72279 - 4.48188 i) \cdot 10^{-14}$	
5	0.246054	$(-1.26793 - 3.76758 i) \cdot 10^{-14}$	
6	0.246016	$(-0.64697 - 3.30274 i) \cdot 10^{-14}$	
\vdots	\downarrow	\downarrow	\downarrow
Limit	0.245911	$(0.34929 - 2.09576 i) \cdot 10^{-14}$	

Table 8: Some weights when interpolating to the $z_c = \frac{1}{2} + \frac{i}{2}$ position using stencils with nodes $z_k = \mu + i\nu$, $-n \leq \mu, \nu \leq n+1$, and n increasing. The analytic limits in the two cases are $\frac{4e^{-\pi/4}\sqrt{\pi}}{\Gamma(\frac{1}{4})^2}$ and $\frac{4}{37}(1-6i)e^{-37\pi/4}\sqrt{\pi}$, respectively.

5.2.2 Case when interpolating to an arbitrary point within a grid square

The evaluation point $\xi = \frac{1}{2}(1+i)$ in (17) is in this case replaced by $\xi = s + it$ with $0 \leq s, t \leq 1$. The counterpart to (17) becomes

$$w_k = \frac{\sigma(s+it)}{((\mu+i\nu) - (s+it)) \lambda_{\mu,\nu}} e^{-\frac{\pi}{2}(\mu(\mu-1)+\nu(\nu-1)+(s+it)(1-i)-2i)}, \quad (20)$$

requiring for all the entries of a PS stencil only one evaluation of $\sigma(s+it)$.

5.3 Brief comment on extrapolation

Just as for real-valued functions, interpolation using equi-spaced data is vastly better conditioned than extrapolation. A famous formula, applicable to both cases, was given by Ramanujan

$$\Gamma(z)f(-z) = \int_0^\infty t^{z-1} \left(f(0) - \frac{t}{1!}f(1) + \frac{t^2}{2!}f(2) - \frac{t^3}{3!}f(3) + \dots \right) dt, \quad (21)$$

valid if $|f(z)| < C e^{A|z|}$ with $A < \pi$ for $\text{Re } z > 0$. A rigorous proof for (21) is contrasted to a heuristic proof and to Ramanujan's original argument in [12], Sections 11.3-11.7.¹⁴ A manifestation of the ill-conditioning is that the RHS of (21) cannot be expressed as a linear combination of the function values $f(0), f(1), f(2), \dots$, but depends on analytic continuation in which these all enter.¹⁵

6 A numerical illustration of complex plane PS approximations

6.1 Some preliminary comment regarding applications

As noted in the Introduction, real axis PS approximations are widely used for various types of PDEs. In the case of time dependent convection-dominated equations, their effectiveness can be heuristically explained by two separate arguments, applying to smooth and to non-smooth data ([7], Sections 4.1 and 4.2, respectively). While certain nonlinear PDEs have solutions that preserve analyticity under time evolution [4, 14, 21], this is generally not the case even for linear PDEs, limiting the range of complex plane PS approximations in the context of PDEs.

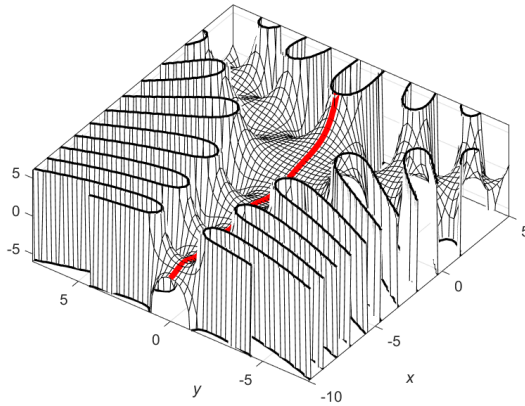
An interesting situation relating to interpolation and derivative approximation arises if complex plane PS approximations are applied to entire functions $f(z)$ which satisfy $|f(z)| < C e^{A|z|^2}$ for some positive constants A and C . Approximating with step size h , the PS weights go to zero faster than the function grows if $h^2 A < \frac{\pi}{2}$, making the PS approximation exact. This is illustrated next in the case of the Airy $\text{Bi}(z)$ function. No matter how large h is used, one can choose an A such that $A < \frac{\pi}{2h^2}$ and then find a C such that $|\text{Bi}(z)| < C e^{A|z|^2}$.

6.2 The Airy $\text{Bi}(z)$ function: Example of a derivative evaluation

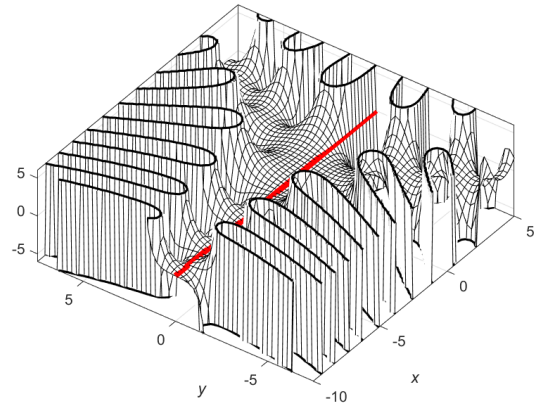
As a numerical demonstration, we consider the Airy $\text{Bi}(z)$ function, illustrated near the origin in Figure 4, and consider the task of approximating $\left. \frac{d}{dz} \text{Bi}(z) \right|_{z=3+2i}$ using complex plane FD formulas with different step sizes h and stencil sizes n (i.e., with $(2n+1) \times (2n+1)$ nodes and, as before,

¹⁴Yet different heuristic arguments leading to (21) can be found in [11], Example 9.32 and Exercise 12.6.6.

¹⁵Numerous mathematical techniques for analytic continuation are described in [11], Chapter 3 and Section 5.3. Numerical methods depend extensively on imposed growth constraints [17, 20].



(a) Real part of $\text{Bi}(z)$



(b) Imaginary part of $\text{Bi}(z)$

Figure 4: Real and imaginary parts of $\text{Bi}(z)$. The real axis is highlighted in red (Reproduced from [11], Figure 11.3).

$n \rightarrow \infty$ representing the PS limit). Figure 5 shows that the error approaches zero extremely rapidly both with decreasing h and increasing n (reflecting how complex plane FD / PS formulas typically would be used).

To test the argument that h can be chosen arbitrarily large and still provide convergence as n increases, we illustrate next the case of $h = 4$. As seen from Figures 6 and 7, the grid now is much too coarse to resolve the rapid oscillations of the Bi-function. Figure 7 show that convergence has been delayed as n increases, but it will still occur.

7 Concluding discussion

FD formulas for a real-valued independent variable are widely used in a variety of contexts, with cost-effectiveness often increasing with their stencil sizes and associated increasing orders of accuracy. Their infinite order PS limit has been extensively studied and used in applications since the 1970's. More recently, PS limits of Hermite-type FD schemes were studied in [1]. Following the introduction of complex plane FD formulas in [10], we have here provided a number of observations on their PS limits. The most striking (and potentially very useful) one is that the PS formulas in this case remain highly local in space, with weights that decay as a Gaussian with the distance from the stencil center point (in sharp contrast to the case with traditional PS approximations).

References

- [1] D. Abrahamsen and B. Fornberg, *On the infinite order limit of Hermite-based finite difference schemes*, SIAM J. Numerical Analysis **59** (2021), no. 4, 1857–1874.
- [2] L.V. Ahlfors, *Complex Analysis*, McGraw-Hill, 1966.
- [3] J.M. Borwein, M.L. Glasser, R.C. McPhedran, J.G. Wan, and I.J. Zucker, *Lattice Sums Then and Now*, Encyclopedia of Mathematics and its Applications, Cambridge University Press, 2013.

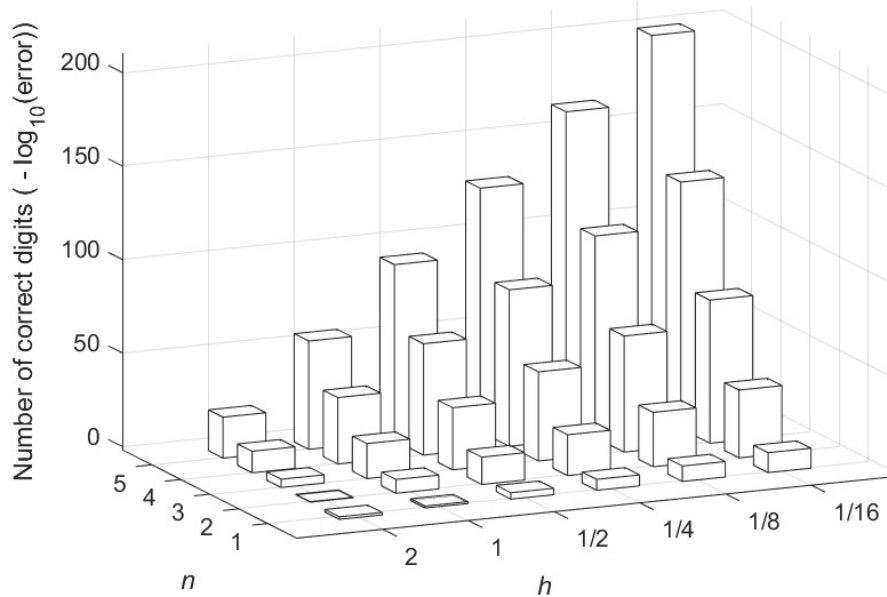


Figure 5: Number of correct digits obtained when approximating $\frac{d}{dz}\text{Bi}(z)|_{z=3+2i}$ using FD stencils of different sizes $(2n + 1) \times (2n + 1)$ and with different step lengths h .

- [4] R.E. Caffisch, F. Gargano, M. Sammartino, and V. Sciacca, *Complex singularities and PDEs*, Riv. Mat. Univ. Parma **6** (2015), 69–133.
- [5] B. Fornberg, *On a Fourier method for the integration of hyperbolic equations*, SIAM J. Numer. Anal. **12** (1975), no. 4, 509–528.
- [6] ———, *Numerical differentiation of analytic functions*, ACM Trans. Math. Software **7** (1981), no. 4, 512–526.
- [7] ———, *A Practical Guide to Pseudospectral Methods*, Cambridge University Press, 1996.
- [8] ———, *Contour integrals of analytic functions given on a grid in the complex plane*, IMA Journal of Numerical Analysis **41** (2021), 814–825.
- [9] ———, *Generalizing the trapezoidal rule in the complex plane*, Numerical Algorithms **87** (2021), 187–202.
- [10] ———, *Finite difference formulas in the complex plane*, Numerical Algorithms **90** (2022), 1305–1326.
- [11] B. Fornberg and C. Piret, *Complex Variables and Analytic Functions: An Illustrated Introduction*, SIAM, Philadelphia, 2020.
- [12] G.H. Hardy, *Ramanujan: Twelve lectures on subjects suggested by his life and works*, Cambridge University Press, 1940, Reprinted by Chelsea Publishing Company, New York, 1978.

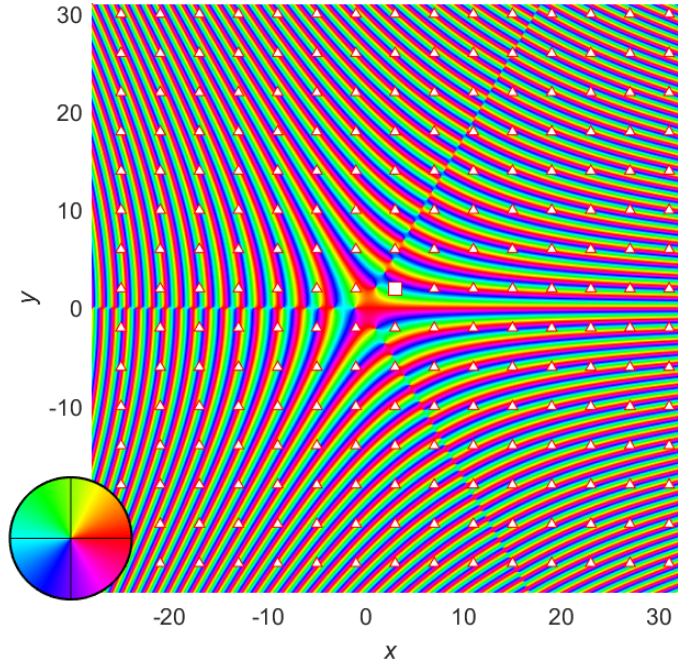


Figure 6: Phase portrait of the $\text{Bi}(z)$ function in a region surrounding the point $z = 3 + 2i$ (white square) at which we wish to approximate $\frac{d}{dz}\text{Bi}(z)$. FD nodes surrounding this point, spaced $h = 4$ apart, are shown as small white triangles, with the displayed node set corresponding to $n = 7$. In this region, the magnitude of $\text{Bi}(z)$ reaches up to around 10^{70} .

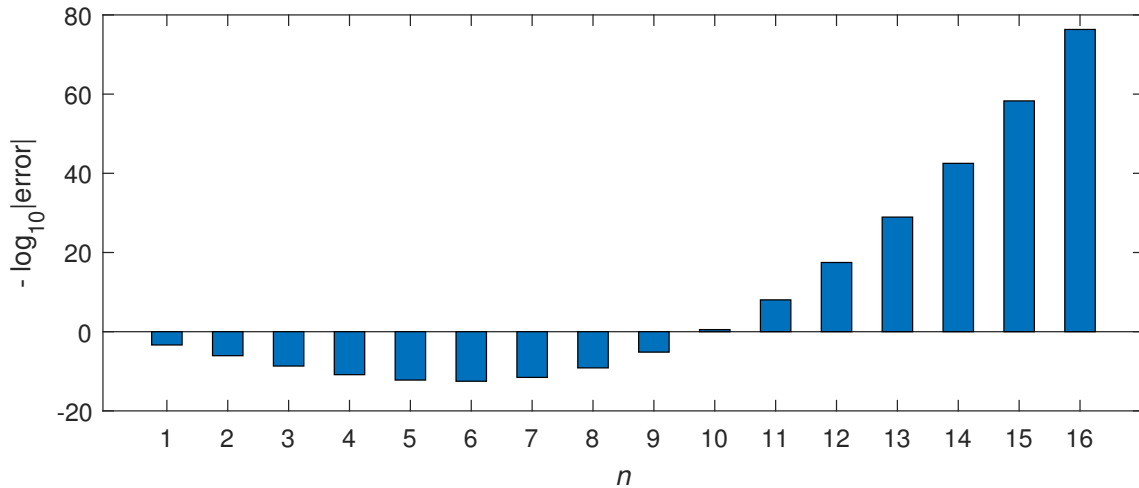


Figure 7: $-\log_{10}|\text{error}|$ when approximating $\frac{d}{dz}\text{Bi}(z)|_{z=3+2i}$ using FD stencils with step length $h = 4$ and of increasing sizes $(2n + 1) \times (2n + 1)$. When positive, $-\log_{10}|\text{error}|$ corresponds to number of correct decimal digits.

- [13] H.-O. Kreiss and J. Oliger, *Comparison of accurate methods for the integration of hyperbolic equations*, *Tellus* **24** (1972), no. 3, 199–215.
- [14] M.D. Kruskal, *The Korteweg-de Vries equation and related evolution equations*, *Lectures in Applied Math. American Math. Soc.* **15** (1974), 61–83.
- [15] J.N. Lyness and C.B. Moler, *Numerical differentiation of analytic functions*, *SIAM J. Numer. Anal.* **4** (1967), 202–210.
- [16] J.N. Lyness and G. Sande, *Algorithm 413-ENTCAF and ENTCRE: Evaluation of normalized Taylor coefficients of an analytic function*, *Comm. ACM* **14** (1971), no. 10, 669–675.
- [17] K. Miller, *Least squares methods for ill-posed problems with a prescribed bound*, *SIAM J. Math. Anal.* **1** (1970), no. 1, 52–74.
- [18] F.W.J. Olver, D.W. Lozier, R.F. Boisvert, and C.W. Clark, *NIST Handbook of Mathematical Functions*, Cambridge University Press, 2010.
- [19] L.N. Trefethen, *Spectral Methods in MATLAB*, SIAM, Philadelphia, 2000.
- [20] ———, *Quantifying the ill-conditioning of analytic continuation*, *BIT Numerical Mathematics* **60** (2020), 901–915.
- [21] J.A.C. Weideman, *Dynamics of complex singularities of nonlinear PDEs: Analysis and computation*, *Recent Advances in Industrial and Applied Mathematics* (T.C. Rebollo, R. Donat, and I. Higuera, eds.), SEMA SIMAI Springer Series, no. ISSN 2199-3041, Springer, 2022.